



## Daily precipitation-downscaling techniques in three Chinese regions

Fredrik Wetterhall,<sup>1,2</sup> András Bárdossy,<sup>3</sup> Deliang Chen,<sup>4,5</sup> Sven Halldin,<sup>1</sup> and Chong-Yu Xu<sup>1,6</sup>

Received 13 September 2005; revised 8 June 2006; accepted 27 July 2006; published 28 November 2006.

[1] Four methods of statistical downscaling of daily precipitation were evaluated on three catchments located in southern, eastern, and central China. The evaluation focused on seasonal variation of statistical properties of precipitation and indices describing the precipitation regime, e.g., maximum length of dry spell and maximum 5-day precipitation, as well as interannual and intra-annual variations of precipitation. The predictors used in this study were mean sea level pressure, geopotential heights at 1000, 850, 700, and 500 hPa, and specific humidity as well as horizontal winds at 850, 700, and 500 hPa levels from the NCEP/NCAR reanalysis with  $2.5^\circ \times 2.5^\circ$  resolution for 1961–2000. The predictand was daily precipitation from 13 stations. Two analogue methods, one using principal components analysis (PCA) and the other Teweles-Wobus scores (TWS), a multiregression technique with a weather generator producing precipitation (SDSM) and a fuzzy-rule-based weather-pattern-classification method (MOFRBC), were used. Temporal and spatial properties of the predictors were carefully evaluated to derive the optimum setting for each method, and MOFRBC and SDSM were implemented in two modes, with and without humidity as predictor. The results showed that (1) precipitation was most successfully downscaled in the southern and eastern catchments located close to the coast, (2) winter properties were generally better downscaled, (3) MOFRBC and SDSM performed overall better than the analogue methods, (4) the modeled interannual variation in precipitation was improved when humidity was added to the predictor set, and (5), the annual precipitation cycle was well captured with all methods.

**Citation:** Wetterhall, F., A. Bárdossy, D. Chen, S. Halldin, and C.-Y. Xu (2006), Daily precipitation-downscaling techniques in three Chinese regions, *Water Resour. Res.*, 42, W11423, doi:10.1029/2005WR004573.

### 1. Introduction

[2] Outputs from general circulation models (GCMs) can be useful in getting an overview of possible climate scenarios but are typically too coarse in scale to be useful in practical comprehensive planning situations, such as applying hydrological modeling in flood-risk analysis. GCMs model precipitation patterns, but the important extreme events are badly represented [Durman *et al.*, 2001]. In many hydrological applications, extreme precipitation patterns such as a number of consecutive rainy days and prolonged dry spells must be well described. Simulations of multisite precipitation series that are to be used in climate change impact studies should thus reproduce the important

patterns in the observed precipitation. One possible solution to overcome this problem is to downscale the output from GCMs to a higher resolution in space/time, thereby making use of scenario output in local water management.

[3] The basic idea of downscaling is to transfer large-scale changes in atmospheric variables (predictors), reliably simulated from GCMs, to local weather series (predictands) [Hanssen-Bauer *et al.*, 2005]. GCM outputs such as mean sea level pressure (MSLP), geopotential heights (GPH), and specific humidity (SH) can be useful predictor variables in statistical downscaling of precipitation in catchment-based studies. Downscaling can be carried with a nested regional climate model (RCM) or differential resolution modeling with GCMs [e.g., Hellström *et al.*, 2001]. Another technique is to apply a statistical link between predictor and predictand. The statistical-downscaling methodology has many obvious drawbacks, such as the uncertain assumption of applicability in a future climate, but it is a computationally cheap and statistically sound complement to dynamical downscaling. Note that predictor and predictand can be the same parameter on different scales, but statistical methods have the freedom to select any variable as predictor as long as it can be motivated.

[4] Several methods of statistical downscaling exist and have been applied in different climate regions [Wilby and Wigley, 1997; Xu, 1999; Linderson *et al.*, 2004]. Although

<sup>1</sup>Air and Water Science, Department of Earth Sciences, Uppsala University, Uppsala, Sweden.

<sup>2</sup>Now at Swedish Meteorological and Hydrological Institute, Norrköping, Sweden.

<sup>3</sup>Institut für Wasserbau, Stuttgart University, Stuttgart, Germany.

<sup>4</sup>Regional Climate Group, Earth Sciences Centre, Göteborg University, Göteborg, Sweden.

<sup>5</sup>Also at Laboratory for Climate Studies/National Climate Center, China Meteorological Administration, Beijing, China.

<sup>6</sup>Now at Department of Geosciences, University of Oslo, Oslo, Norway.

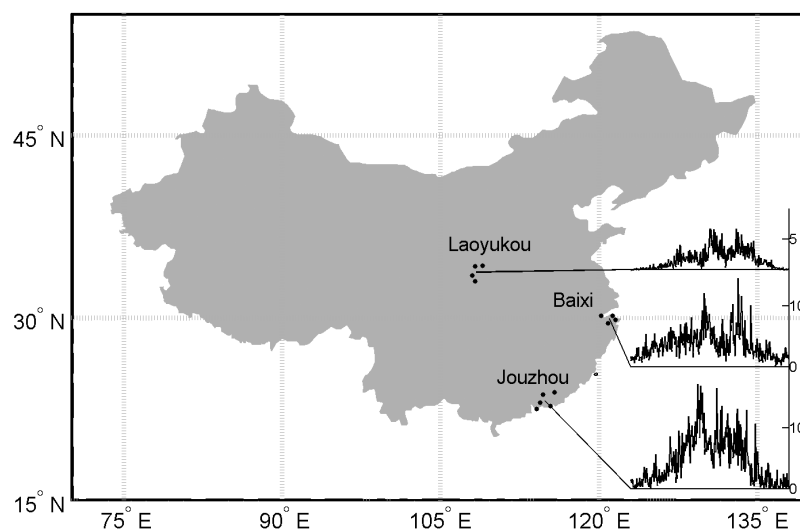


**Figure 1.** Map of mainland China with the location and annual cycle (January–December) of mean daily precipitation for the stations used. The amounts (millimeters) are averaged over the period 1961–2000 for all stations in each area.

several comparative studies have been carried out in Europe [Wilks and Wilby, 1999; Beckmann and Buishand, 2002; Stehlik and Bárdossy, 2002; Wetterhall et al., 2006], the methods used have only been tested in climates where they were developed. It is important to identify the strengths and weaknesses of different statistical-downscaling methods to understand under which conditions they can be applied, such as time of year and spatial domain of the predictor data. However, compared with the rich studies performed in the United States and European countries, few statistical-downscaling exercises have been carried out in the Chinese context [Chen and Chen, 2003; Liao et al., 2004]. While studies for single station and single method in China have appeared [e.g., Jia et al., 2006], no study has been reported that compares different downscaling methods in different climatic regions of China [Fan et al., 2006]. This study is thus the first to evaluate the performance of different statistical-downscaling methods in eastern, southern, and inland China. The comparison is important if the uncertainty of statistical downscaling of precipitation concerning predictors and methodology is to be evaluated [Chen et al., 2006].

[5] The precipitation pattern in China is strongly governed by the East Asian Monsoon, which brings moist, warm air in summer and dry, cool air during winter, creating a strong variation in the annual precipitation cycle [e.g., Ding, 1994]. The summer precipitation amount decreases with latitude and distance from the coast, resulting in the largest precipitation amounts in the southeast and the driest climate in the northwest and the Tibetan Plateau. The start date of the summer monsoon is later with increasing latitude (Figure 1). The circulation patterns that govern precipitation distribution work on a very large scale; therefore the selection of predictor in terms of spatial and temporal domain imposes a great challenge for any downscaling study in China [Samel et al., 1999]. The interannual variability of total rainfall in China during summer also has a strong relationship to the Eurasian circulation [Samel et al., 1999]. Further understanding of the link between

large-scale circulation patterns and local precipitation is thus essential for assessing the possible effects of a global climate change on water resources in China.

[6] The purpose of this study was therefore twofold. The first aim was to analyze and model the seasonal relationship between large-scale circulation and precipitation in the three regions in China with four statistical-downscaling methods. The second aim was to compare the ability of the four methods to downscale extreme events and intra-annual variation in order to find the best suited model for each of the three catchments, depending on season.

## 2. Study Area and Data

### 2.1. Study Areas

[7] The study region consists of three catchments in southern, eastern, and central China (Figure 1). The areas were selected to represent three different climates; subtropical with heavy monsoon precipitation in the south (Jouzhou), intermediate monsoon to the east (Baixi), and inland temperate climate in central China (Laoyukou). The three areas are subcatchments to the three largest rivers in China, the Yangtze River (Baixi), the Yellow River (Laoyukou), and the Pearl River (Jouzhou). The precipitation in China has a seasonal cycle, with the largest precipitation amounts falling during the summer months because of the monsoon circulation (Figure 1), but the amounts are strongly dependent on the direction of moisture flux from the South China Sea [Simmonds et al., 1999].

### 2.2. Data

[8] The predictands are daily precipitation data (1961–2000) from four weather stations inside or within a 100-km distance of Baixi and Laoyukou catchments each, and five weather stations inside or within a 100-km distance of Jouzhou catchment. The observed daily precipitation data were provided by the National Climate Centre of China, and the quality of the records was controlled. All station records used in the analysis have complete series for the whole time

**Table 1.** Precipitation Stations in the Three Catchments in China<sup>a</sup>

Station ID	Latitude	Longitude	Meters Above Sea Level	Precipitation, mm
<i>Laoyukou</i>				
57034	34°15′	108°13′	448	623
57036	34°18′	108°56′	398	574
57134	33°32′	107°59′	1088	942
57232	33°3′	108°16′	485	908
<i>Baixi</i>				
58457	30°14′	120°10′	42	1376
58467	30°12′	121°16′	4	1257
58556	29°36′	120°49′	104	1286
58562	29°52′	121°34′	5	1373
<i>Jouzhou</i>				
59501	22°48′	115°37′	17	1869
59298	23°5′	114°25′	22	1716
59293	23°44′	114°41′	41	1933
59493	22°33′	114°6′	18	1873
59303	23°56′	115°46′	121	1495

<sup>a</sup>Precipitation values (millimeters) are given as annual averages for 1961–1990.

period. The precipitation amount is expressed as millimeters per day throughout this paper, unless something else is expressed explicitly. A summary of the station data is given in Table 1. The predictor variables were large-scale grid-point data of MSLP, geopotential height at 1000, 850, 700, and 500 hPa (H1000, H850, H700, and H500), wind speed and direction (U/V850, U/V700, U/V500), and specific humidity (S850, S700, S500) from the National Centers for Environmental Prediction/National Center for Atmospheric Research (NCEP/NCAR) reanalysis project [Kalnay *et al.*, 1996] (<http://dss.ucar.edu/pub/reanalysis/>). All predictors were evaluated, but only a few were ultimately selected for each method and region.

### 3. Methods and Model Setup

#### 3.1. Analogue Method

[9] The analogue method models precipitation in two steps. The first step is to analyze characteristics of the large-scale circulation that are relevant for the predictand precipitation to optimize the temporal and spatial domain of the predictor. Second, the target predictand at a certain time  $t$  is simulated by selecting an historic event  $F(u)$  based on similarities of certain characteristics in the predictor  $F(t)$  field using equation (1):

$$\min \| \mathbf{F}(u) - \mathbf{F}(t) \|, \quad (1)$$

where the target predictand is the historic event that minimizes the difference. The predictand can be extended to an ensemble of events by selecting not only the one historic event, but a number of events that give lowest values for equation (1).

[10] There exist a number of techniques to analyze the predictor field. In this paper, the principal component analysis method (PCA) and Teweles-Wobus scores (TWS) were applied. PCA analyzes anomalies of the predictor series where the long-term mean, trend, and seasonality have been removed. The application of PCA as an analogue method has been outlined by Zorita and von Storch [1999].

The TWS method uses a measure of the differences in gradients of the large-scale predictor field to select the analogue. Obled *et al.* [2002] presented an application of TWS in the analogue method for precipitation downscaling. The methods have been applied on a catchment in central Sweden by Wetterhall *et al.* [2005, 2006].

#### 3.2. Multiobjective Fuzzy-Rule-Based Classification Method

[11] The weather pattern method is a multiobjective fuzzy-rule-based classification method (MOFRBC) that has been applied to a number of areas in Europe, i.e., Germany [Bárdossy *et al.*, 2001], Germany and Greece [Stehlik and Bárdossy, 2002], mainland Europe [Stehlik and Bárdossy, 2003], and Sweden [Wetterhall *et al.*, 2006]. The method identifies and classifies large-scale circulation patterns from a gridded predictor using fuzzy rules [Bárdossy *et al.*, 1995]. The classification patterns (CPs) are objectively and automatically optimized on precipitation using simulated annealing [Bárdossy *et al.*, 2001]. The optimization derives circulation patterns that explain precipitation patterns (dry and wet conditions), and this is achieved by maximizing two objective functions, describing precipitation occurrence ( $I_1$ ) and amount ( $I_2$ ) for a specific pattern,

$$I_1 = \frac{1}{T} \sum_{t=1}^T |p(CP(t)) - \bar{p}| \quad (2)$$

$$I_2 = \frac{1}{T} \sum_{t=1}^T \left| \ln \left( \frac{z(CP(t))}{\bar{z}} \right) \right|, \quad (3)$$

where  $T$  is the number of classified days,  $p(CP(t))$  is the probability of precipitation on day  $t$  assuming that the circulation pattern is known and equal to  $CP(t)$ ,  $\bar{p}$  is the probability of precipitation for all days,  $z$  is the mean precipitation amount on day  $t$  with classification  $CP(t)$ , and  $\bar{z}$  is the mean precipitation amount for all days.

[12] The precipitation model is dependent on the circulation pattern and calendar day  $t^*$ . The model will only be briefly introduced here; for a more extensive explanation, see Bárdossy and Plate [1992], Bárdossy *et al.* [2001], and Stehlik and Bárdossy [2003]. Let  $A = \{\alpha_1, \dots, \alpha_n\}$  be the set of atmospheric patterns from where the observed atmospheric pattern  $A_t$  is taking its value. The modeled precipitation amount  $Z$  at time  $t$  and point  $u$  is a random function

$$Z(t, u) = \begin{cases} 0 & \text{if } (W(t, u) \leq 0) \\ W^\beta(t, u) & \text{if } (W(t, u) > 0), \end{cases} \quad (4)$$

where  $W(t, u)$  is a normally distributed random function, with mean  $\mu$  and standard deviation  $\sigma$ , for any location  $u$ . The parameter  $\beta$  is a positive exponent that skews  $W^\beta(t, u)$  to fit the precipitation distribution. This approach links the discrete-continuous distribution  $Z(t, u)$  to a normally distributed function that makes it easier to model multivariate processes. The distribution of precipitation at a certain location is CP dependent. In a recent development, moisture flux was included in the model (W. Yang *et al.*, manuscript in preparation, 2006), and therefore this part will be

**Table 2.** Abbreviations of Indices Used to Evaluate the Results<sup>a</sup>

Index	Abbreviation
Ranked-probability score	RPS
Continuous ranked-probability score	(C)RPS
Average wet day amount, mm	wetday
Largest 5-day total rainfall, mm	max5
Maximum length of dry spell, days	maxdry
Ninetieth-percentile-of-rain-day amounts, mm/d	90perc
Number of days exceeding long-term 90th percentile, days	90days
Percentage of days long-term exceeding 90th percentile	90amount

<sup>a</sup>All indices except the (C)RPS are suggested by the STARDEX [2001] project.

described more in detail. Moisture flux is defined as geostrophic wind multiplied by the specific humidity. The distribution parameters  $\mu$  and  $\sigma$  of the CP-dependent Gaussian distribution  $W(t,u)$  are replaced by the parameters  $\mu_i$  and  $\sigma_i$ , defined as

$$\mu_i(t,u) = \mu_0 + a^*MF(t,u) \quad (5)$$

$$\sigma_i(t,u) = \sigma_0, \quad (6)$$

where  $MF$  is the daily moisture flux,  $a^*$  is a coefficient from the linear relationship between  $MF$  and precipitation, and  $i$  denotes the classification. The expected value of precipitation is therefore dependent on both CP and time of year. The random process  $W(t,u)$  is defined as

$$W(t,u) = r(t^*)(W(t-1,u) - W_i(t^*-1,u)) + C_i(t^*,u)\Psi(t,u), \quad (7)$$

where  $r(t^*)$  is the autocorrelation for 1-day time lag,  $i'$  is the CP on day  $t-1$ ,  $C_i(t^*,u)$  is a matrix of spatial and space-time covariations, and  $\Psi(t,u)$  is a random vector of independent normalized random variables. The autocorrelation function is independent on the circulation pattern, but dependent on the annual cycle, which in turn is approximated by a Fourier series, usually with three parameters. The parameter estimation of equations (5)–(6) is done by the maximum likelihood method.

### 3.3. Statistical Downscaling Method

[13] The statistical downscaling model (SDSM) [Wilby et al., 1999, 2002] is a hybrid between a multilinear regression method and a stochastic weather generator. Large-scale predictors are used to linearly condition local-scale weather generator parameters. The model has been applied in many catchments in North America [Wilby and Dettinger, 2000] and Europe [Wilby et al., 2002; Wetterhall et al., 2006]. The method is generally described as [Wilby et al., 2003]

$$\omega_t = \alpha_0 + \sum_{j=1}^n \alpha_j \hat{u}_t^{(j)}, \quad (8)$$

where  $\omega_t$  is the conditional probability of precipitation occurrence on day  $t$ ,  $\hat{u}_t^{(j)}$  are the normalized predictors, and

$\alpha_j$  are the estimated regression coefficients. Precipitation occurs if  $\omega_t \leq r_t$ , where  $r_t$  is a computer-generated uniformly distributed stochastic number. The precipitation amount given that precipitation occurs is modeled by

$$Z_t = \beta_0 + \sum_{j=1}^n \beta_j \hat{u}_t^{(j)} + \varepsilon, \quad (9)$$

where  $Z_t$  is the z-score for day  $t$ ,  $\beta_j$  are estimated regression coefficients calculated for each month,  $\varepsilon$  is a normally distributed stochastic error term, and

$$y_t = F^{-1}[\phi(Z_t)], \quad (10)$$

where  $\phi$  is the normal cumulative distribution function and  $F$  is the empirical distribution function of the  $y_t$  daily precipitation amounts. It can be noted that the same predictors are used to model precipitation occurrence and amounts and that the predictors are normalized over the period 1961–1990.

### 3.4. Evaluation

[14] The simulated rainfall was evaluated by calculating extreme precipitation indices as stipulated by the Statistical and Regional dynamical Downscaling of Extremes for European regions (STARDEX) project [Frei, 2001] (Table 2). The indices were used to assess the ability of the methods to downscale extreme events, which are of interest in climate impact assessments. If the models are to be used in climate change studies, the interannual variability has also to be reasonably well modeled; otherwise the models lack in sensitivity to climate variability and the usefulness in climate change studies can be questioned. Therefore the annual rainfall, ranked probability scores (RPS) [Epstein, 1969; Murphy, 1971; Obled et al., 2002] of precipitation and continuous ranked probability scores (CRPS) [Hersch, 2000] for the seasonal STARDEX indices were also used to compare the methods.

[15] The probability scores are commonly used to evaluate forecasts [Jolliffe and Stephenson, 2003] and are calculated by classifying a random variable  $X$  with  $K$  ( $>2$ ) thresholds,  $x_1 < x_2 < \dots < x_K$ , that defines the events  $A_k = \{X \leq x_k\}$  for  $k = 1, 2, \dots, K$  with the forecast probabilities  $(\hat{p}_1, \hat{p}_2, \dots, \hat{p}_K)$ . The binary indicator variable for the  $k$ th event is denoted  $o_k$  and defined as  $o_k = 1$  if  $A_k$  occurs and 0 otherwise,

$$RPS = \frac{1}{N} \frac{1}{K} \sum_{n=1}^N \sum_{k=1}^K (\hat{p}_k(n) - o_k)^2 \quad (11)$$

$$CRPS = \frac{1}{N} \sum_{n=1}^N \int_{-\infty}^{\infty} [F(x(n)) - H(x(n) - x_0)]^2 dx, \quad (12)$$

where  $x(n)$  is the  $n$ th forecast of the  $N$  number of forecasts and  $x_0$  is the observed value. The  $CRPS$  is the continuous extension of  $RPS$  where  $F(x)$  is the cumulative distribution function (CDF)  $F(x) = p(X \leq x)$  and  $H(x - x_0)$  is the Heaviside function, which has the value 0 when  $x - x_0 < 0$

and 1 otherwise. In order to quantify the skill of the probability score, the skill score is calculated as

$$SS_{(C)RPS} = 1 - \frac{(C)RPS_{FP}}{(C)RPS_{RP}}, \quad (13)$$

where  $(C)RPS_{FP}$  denotes the forecast score and  $(C)RPS_{RP}$  is the score of a reference forecast of the same predictand. The  $(C)RPS$  is a verification tool that compares how the distribution of an ensemble of forecasts predicts the observed value, and it is sensitive to bias as well as variability in the forecasted values. A skill score  $SS_{(C)RPS}$  close to unity means a successful simulation; if the skill score is negative, the method is performing worse than the reference forecast.

[16] For the seasonal STARDEX indices the reference forecast was stochastically resampled precipitation for each season generated from the observed data by selecting analogues randomly from the historical database. The reference forecast for  $RPS$  was a persistence forecast, i.e., the precipitation on day  $t$  was the observed precipitation on day  $t - 1$ . The thresholds for  $RPS$  were the observed precipitation percentiles at 90, 95, 98, 99, 99.5, and 100 in order to represent the extreme precipitation events rather than the mean values. The arithmetic means of the STARDEX indices were tabulated to identify possible biases. Persistence forecasts are more useful in climate studies since they preserve the statistical properties of the predictand, but since this would yield negative values for the STARDEX skill scores indices using the analogue methods, this reference forecast was only possible for  $RPS$ . Also, the correlation coefficient for seasonal total precipitation was used as an indicator of the methods' ability to capture interannual variations in seasonal total amount of precipitation.

### 3.5. Model Setup

[17] The methods were calibrated and validated by split-sample test, using 25 years for calibration (1961–1978, 1994–2000) and 15 years for validation (1979–1993), deliberately selecting the same time periods as those proposed by the STARDEX project. This makes the study comparable with other studies carried out in Europe [STARDEX, 2001; Wetterhall et al., 2006]. The analysis was also divided into two seasons, one summer season stretching from April to September and one winter season from October to March. This seasonality follows the intra-annual variability of the monsoon, with southwesterly winds bringing moisture in summer and northeasterly drier winds in winter. The interannual variability of the timing and magnitude of the monsoon rain season is large, and the analysis was carried out both on annual, seasonal, and daily statistics of the precipitation. In order to study the relative importance of the moisture flux, two of the methods, SDSM and MOFRBC, were applied in two modes, one using only MSLP and/or geopotential heights (H850 and H700) as predictors and one adding moisture flux or specific humidity as a predictor (SDSMh and MOFRBCh). The analogue methods were only applied in the first mode. The motivation for this restriction was to limit the number of model setups.

[18] The spatial coverage of the predictors was evaluated by varying the spatial domain of the predictor data for all

catchments and seasons. The temporal domain was restricted by imposing a time window on the predictor. The time window prohibits analogues from a totally different season to be selected as the target predictand. For example, if the target predictand was 1 June and the time window 8 days, the available analogues in the historical database were limited to dates between May 24 and 9 June for all years. The optimum setting was selected by calculating an unweighted objective function of the sum of the normalized values of  $RPS$  and the STARDEX indices over the calibration period,

$$O(j, k) = \sum_{t=1}^T \sum_n^N |s(j, k)_{t,n} - o_{t,n}|, \quad (14)$$

where  $s$  is the simulated and  $o$  is the observed normalized objective functions ( $RPS$  and STARDEX) for season  $t$  and station  $n$ . The objective function was calculated for different spatial domains  $j$ , and time windows  $k$ , ranging from 1 to 60 days. The predictor setting that minimized the objective function was selected as the predictor. Since the analogue methods are deterministic, the creation of an ensemble of forecasts was achieved with a selection scheme,

$$\bar{F} = \left\{ [F(i, j)]_{j=0}^{i=-7, \dots, +7}, [F(i, j)]_{j=-1}^{i=-3, \dots, +3}, [F(i, j)]_{j=+1}^{i=-3, \dots, +3}, F(0, 0) \right\}, \quad (15)$$

where  $\bar{F}$  denotes the ensemble of the 30 forecasts  $F(i, j)$  with the spatial window  $j$  and temporal window  $i$ . The optimum window is at  $i = j = 0$ , and  $j = \pm 1$  denotes the  $l$  spatial, and  $i = \pm n$  denotes the  $n$  time windows, closest to the optimum window.

### 3.6. Using MSLP and/or Geopotential Heights as Predictors

[19] The predictor set for the SDSM method was screened by forward stepwise multilinear regression of all predictors for each catchment and season in the daily precipitation series adding predictors that improved the model on a significance level of 0.001, and removing predictors on the significance level 0.1. The model was then built in the SDSM interface with the selected predictors from the first step. The stringent significance level in the first step was selected to restrain the number of predictors going in to the model. The model has the ability to modify the results in terms of bias and inflation and the optimum settings for each station were calibrated manually using the objective function (equation (14)) as indicator of model performance. The objective functions used in the optimization of MOFRBC (equations (2)–(3)) yield very wet/dry rather than intermediate weather, since they give high values for classifications that are either really wet or dry. The classification with the highest  $I_1$  and  $I_2$  were selected as the best. Precipitation and normalized ranked precipitation were used as predictands in the optimization of the circulation patterns.

### 3.7. Adding Moisture Flux or Specific Humidity as a Predictor

[20] In the second mode, moisture flux was considered as an additional predictor for MOFRBC and SDSM. In the

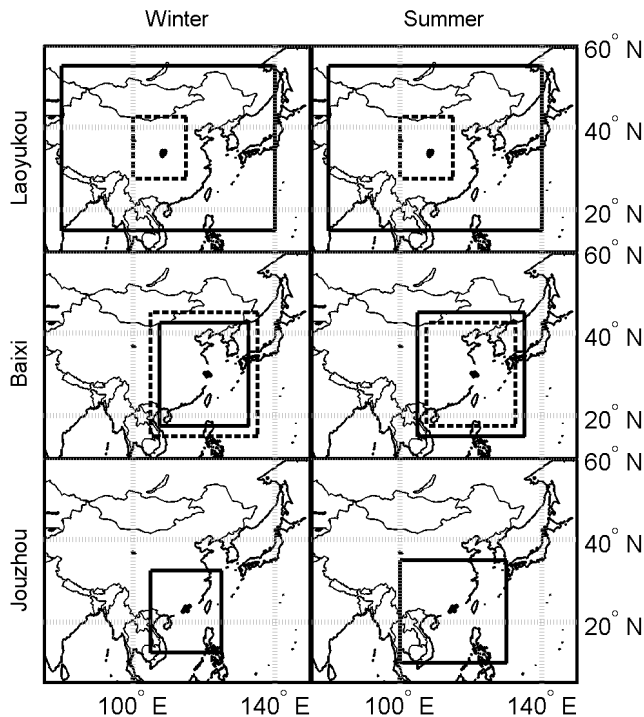


**Figure 2.** Optimum spatial windows for the analogue methods for summer and winter season. The solid lines are the principal components analysis (PCA) method, and dotted lines are the Teweles-Wobus scores (TWS) method. For Jouzhou the optimum areas coincide.

case of SDSMh, S850, S700, and S500 as well as U/V850, U/V700, and U/V500 were added to the predictor set using the same methodology as above. For the MOFRBC method the moisture flux was used to modify the precipitation model by adjusting the parameters (equation (5)). The moisture flux was defined as specific humidity multiplied by wind speed in  $u$  and  $v$  directions at the levels 850, 700, and 500 hPa. The analysis was carried out seasonally for grid points closest to each catchment in order to find the moisture flux direction with highest correlation with precipitation.

## 4. Results

### 4.1. Analogue Methods

[21] The five leading principal components (PCs) were used to select analogues for the PCA method, which explained 75–90% of the variance of the MSLP field depending on station and extent of the predictor field. The cutoff at five PCs was selected after plotting the eigenvalues and keeping the PCs above the threshold for which the explained variance did not increase substantially. The screening of best large-scale predictor resulted in MSLP for the analogue methods with different spatial and temporal windows depending on catchment and season (Figure 2, Table 3). It is seen from Figure 2 and Table 3 that (1) for all catchments the spatial window was of similar size independent of season and method, except for the Laoyukou catchment, where the optimum spatial window was much larger for PCA than for TWS, and (2) as for the time window, significant differences existed between seasons,

methods, and catchments. The largest variation in predictor settings was found for Laoyukou catchment, and the smallest variation was found for Baixi catchment.

### 4.2. SDSM Method

[22] MSLP was chosen as predictor for SDSM according to the results from the predictor evaluation. A screening of the relationship between MSLP and precipitation gave different results depending on season and catchment (Figure 3). It is seen that (1) the Spearman ranked correlation coefficient between MSLP and precipitation was much larger during winter than during summer for all catchments; (2) the grid points with largest negative correlation for Baixi and Jouzhou were outside the coast, whereas the area was stretching farther inland for Laoyukou; (3) the summer pattern was similar to the winter patterns but the correlation was much weaker for summer; and (4) the selected predictor points for SDSM were more centered over the study area for Laoyukou in summer, but this was not the case for the other catchments. Specific humidity and wind speed were the most selected parameters from the stepwise multiple regression for the SDSMh. The only case where MSLP was clearly important was for Baixi in wintertime.

### 4.3. MOFRBC Method

[23] The optimum predictor for MOFRBC was MSLP at all catchments, although the difference was not very large when using H850 or H700 as predictor. The classification also improved in terms of  $I_1$  and  $I_2$  (equations (2) and (3)) when using the weather patterns that were optimized using ranked precipitation for the coastal catchments Baixi and Jouzhou. The reason to use ranked precipitation is to improve classification by removing the skewness of the distribution of daily precipitation amounts. For these catchments, separate classifications were used for summer and winter since an optimized classification for the whole year was not attainable. Splitting the classification in two seasons disrupted the lagged autocorrelation of the precipitation model (equation (7)). However, since the evaluation of the STARDEX indices was done seasonally, this was not considered a major problem. For Laoyukou the same classification was used for both seasons. The  $I_1$  and  $I_2$  were generally lower for this region than for the other two.

[24] The optimum spatial window for each region was quite large and always centered over the precipitation stations (Figure 4). Figure 4 also shows that (1) the wet summer and dry winter patterns varied depending on catchment; (2) the dry and wet patterns for the southerly catchments (Baixi and Jouzhou) were similar for wintertime, with wet conditions caused by a negative anomaly pattern centered directly over the area. The wet pattern for Laoyukou was instead a strong bipolar structure, caused by geostrophic winds from southeast; (3) the dry patterns for Baixi and Jouzhou were almost the mirror images of the wet

**Table 3.** Optimum Time Windows for the Analogue Methods

Method	Laoyukou		Baixi		Jouzhou	
	Winter	Summer	Winter	Summer	Winter	Summer
TWS, days	10	10	25	25	20	25
PCA, days	40	20	25	20	15	30

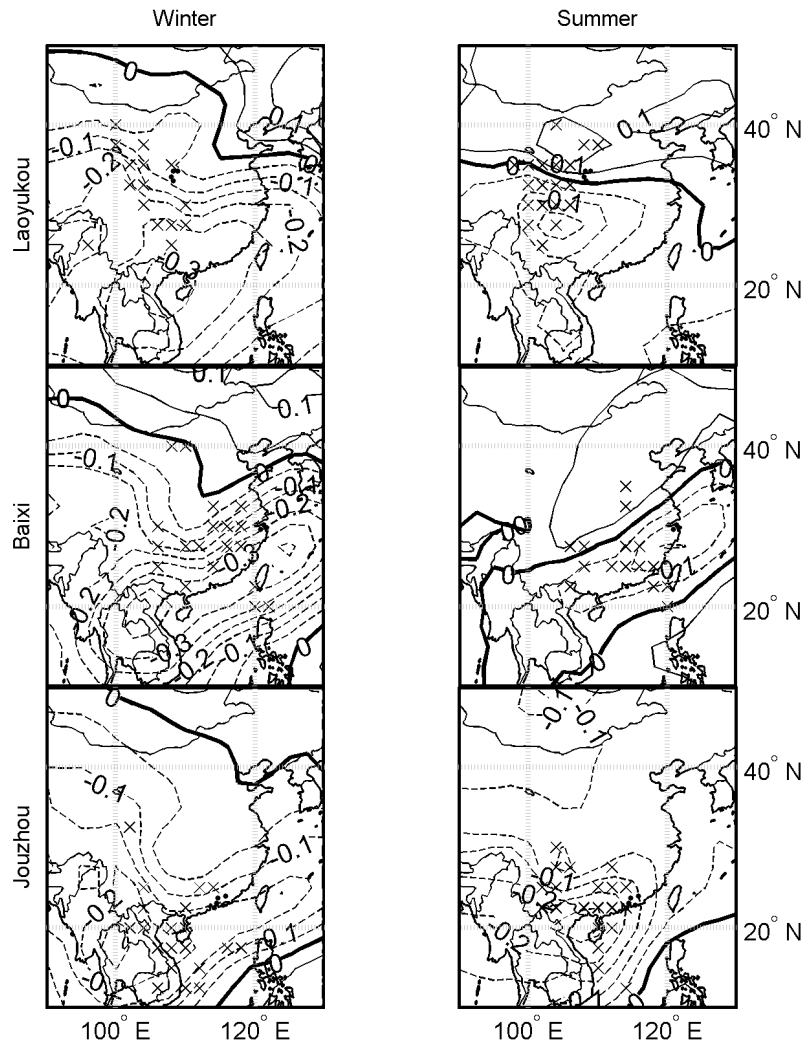


**Figure 3.** Isolines of ranked correlation between mean sea level pressure (MSLP) and precipitation for three catchments. Dashed lines denote negative, solid lines denote positive, and the bold line denotes zero correlation, whereas crosses denote the grid points used in the statistical downscaling model (SDSM).

for the winter classification, with a strong positive anomaly on the sea south/southwest of the catchment; (4) the dry pattern for Laoyukou was similar to the wet pattern, but the negative anomaly was deeper and stretched farther north; and (5) the wet patterns for summer had similar structure for all catchments with a bipolar anomaly field that is rotating anticlockwise as it moves northward. At Laoyukou the negative anomaly is located west of the catchment with a positive ridge in the north. For Baixi, the negative anomaly has moved north and the positive anomaly has moved south, creating bipolar structure. Finally, at Laoyukou, a negative anomaly is located far north and the positive anomaly is located to the southeast. No resemblance between the dry patterns was recognizable.

#### 4.4. STARDEX Indices

[25] The statistical properties averaged over seasons and catchments for the evaluation period were quite well captured for all methods and seasons (Table 4, Figure 7). The models generally performed worse during summer than winter with some differences between indices. For example,

*max5* was better downscaled for the summer season. The best performance for all methods were for the southerly catchments during winter, with the exception for *max5*, and the overall performances of the more complicated methods were better than the analogue methods. MOFRBCh was the best method during winter season, and SDSMh was best for Jouzhou and MOFRBC for Baixi during the summer season. MOFRBC also captured *maxdry* best for winter.

#### 4.5. Timing and Amount of Precipitation

[26] The occurrence and amount of daily precipitation were best captured by SDSM and SDSMh, but also MOFRBC outperformed the analogue methods for all seasons and catchments (Table 5). The modeling of the seasonal cycle was improved in the MOFRBCh and especially for the SDSMh compared with MOFRBC and SDSM (Figure 5). MOFRBCh modeled the start of the summer monsoon too early and underestimated the cyclonic precipitation of the late summer. Both SDSM models and TWS captured the interannual variability (both *RPS* and correlation) quite well for Laoyukou (Table 5). SDSM captured the

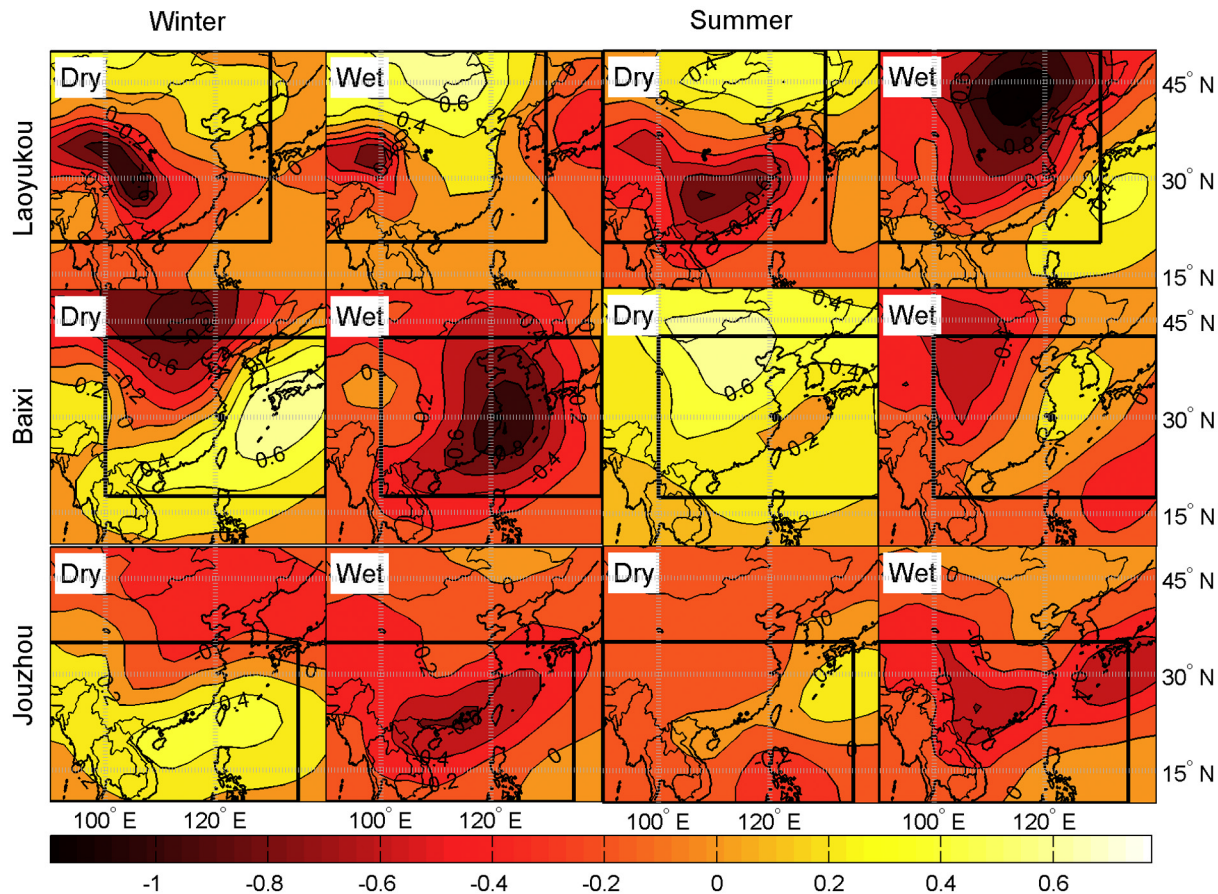


**Figure 4.** Composite maps of normalized MSLP anomalies for the driest and wettest circulation patterns classified with the multiobjective fuzzy-rule-based classification method (MOFRBC/MOFRBCh). The boxes indicate the optimum spatial window for each region.

interannual variability well also for Baixi and Jouzhou, although the correlation coefficient for summer decreased farther to the south. The opposite was apparent for the MOFRBC models, which totally missed the interannual variability for Laoyukou (although a reasonable correlation coefficient of 0.48 was obtained for MOFRBCh in summer), but managed quite well in the southerly catchments (highest correlation coefficients were found for MOFRBCh for both seasons).

[27] The spatial correlation of daily precipitation did not decrease so drastically with distance (Figure 6). The MOFRBCh preserved the correlation structure better than SDSMh, but SDSM models have the apparent disadvantage in spatial correlation since each station was modeled separately with a large stochastic component added to each time series (equation (9)). The spatial correlation was higher for winter than for summer. The most southerly catchment (Jouzhou) had the lowest correlation for both winter and summer. Since no additional data about the locality of the precipitation stations were available, no conclusion could be drawn about this behavior.

## 5. Discussion

### 5.1. Predictor Selection

[28] In order to compare the methods as objectively as possible the predictor setting was restricted to only MSLP in

the first mode of the MOFRBC and SDSM. In the case of MOFRBC, also H850 and H700 were evaluated as predictors, but the optimum classification was achieved with MSLP as predictor. This could be because MSLP incorporates near-surface variations to a higher extent than geopotential heights. MOFRBCh included moisture fluxes at 850, 700, and 500 hPa levels, so in order to make SDSMh as comparable as possible in terms of the available predictor set, specific humidity, geostrophical winds, and geopotential height at the same levels were added to represent the moisture flux in this mode. The predictor set could thus be increased for SDSM, but the focus here was to make the two methods comparable. The consequence of the different spatial windows for the analogue methods in the Laoyukou catchment was that PCA incorporates MSLP variations in the China Sea, whereas TWS only captures gradients just above the study area. The predictor optimization for this area was the most difficult to evaluate, and this may indicate that the methods did not capture processes that are important for precipitation sufficiently. A thorough study of the local processes governing precipitation might give better results.

[29] There were large similarities in the classification patterns for MOFRBC and SDSM predictor variables for winter. The extreme circulation patterns for MOFRBC at Baixi and Jouzhou had their centers outside the coast of the catchment area although with opposite anomaly signs

**Table 4.** STARDEX Indices for the Three Catchments; Average Over All Stations for the Validation Period

	Obs	PCA	TWS	MOFRBC	MOFRBCh	SDSM	SDSMh
<i>Laoyukou</i>							
Winter (Oct–Mar)							
wetday, mm	3.4	4.1	3.3	4.6	4.1	4.0	4.0
max5, mm	41	44	41	51	49	56	54
maxdry, days	31	24	27	28	26	21	22
90perc, mm/d	10.0	11.5	8.9	12.3	10.8	11.0	11.3
90days, days	16	18	17	19	21	19	21
90amount	0.86	0.90	0.87	0.91	0.90	0.89	0.89
Summer (Apr–Sep)							
wetday, mm	8.45	8.40	8.43	9.59	7.68	8.86	8.55
max5, mm	104	100	110	106	93	115	107
maxdry, days	11	11	11	15	13	10	11
90perc, mm/d	24	23	23	25	20	24	23
90days, days	21	20	21	20	20	24	22
90amount	0.78	0.78	0.77	0.78	0.71	0.78	0.77
<i>Baixi</i>							
Winter (Oct–Mar)							
wetday, mm	6.3	5.7	5.9	6.7	6.6	5.7	5.4
max5, mm	80	70	70	82	85	80	75
maxdry, days	21	12	15	19	18	12	13
90perc, mm/d	17	15	16	17	17	15	15
90days, days	8.1	7.9	7.5	7.3	8.5	7.8	7.6
90amount	0.44	0.44	0.43	0.42	0.42	0.46	0.43
Summer (Apr–Sep)							
wetday, mm	10.9	10.6	10.9	11.7	10.1	11.7	11.5
max5, mm	141	140	158	146	137	174	181
maxdry, days	13	8.3	9.8	14.0	12.3	11.1	10.5
90perc, mm/d	30	29	29	30	26	30	29
90days, days	10	9.9	10	8.6	7.8	10	11
90amount	0.47	0.47	0.50	0.44	0.34	0.52	0.49
<i>Jouzhou</i>							
Winter (Oct–Mar)							
wetday, mm	7.36	7.28	5.51	8.59	7.38	6.01	5.72
max5, mm	108	101	74	84	95	82	85
maxdry, days	34	20	28	32	22	20	18
90perc, mm/d	21	20	16	23	19	17	16
90days, days	6.9	5.9	3.8	5.1	7.2	4.9	5.7
90amount	0.58	0.61	0.45	0.53	0.46	0.53	0.50
Summer (Apr–Sep)							
wetday, mm	15.4	14.8	14.7	17.1	15.46	15.9	15.7
max5, mm	260	227	234	219	222	259	272
maxdry, days	11	8.5	8.3	16	13	10	8.8
90perc, mm/d	42	41	42	44	39	43	43
90days, days	9.8	8.8	9.7	7.9	7.9	9.1	11.4
90amount	0.49	0.46	0.47	0.40	0.35	0.50	0.50

(Figure 4). Very similar patterns were shown in the correlation pattern and in the selected predictor points for SDSM. For Laoyukou the similarity was not as striking, but the fields were similar. This indicates that the methods identify the same predictor area as being important for winter precipitation. For summer the patterns differed more, which indicated that the summer precipitation is governed by a more complex large-scale circulation and/or more local factors.

## 5.2. STARDEX Indices

[30] The  $SS_{(C)RPS}$  revealed that the indices were not overall successfully modeled for Laoyukou, and often worse than the reference simulation except for *maxdry* in winter (Figure 7). This was not evident in the STARDEX indices (Table 4), and the reason for this was that  $SS_{(C)RPS}$  evaluates the timing and distribution of extreme events rather than the seasonally averaged values. For the two southerly catchments all methods performed much better,

and here the two complicated methods outperformed the analogue methods for all seasons. The skill scores for winter precipitation were generally higher than for summer precipitation for Jouzhou and Baixi catchments (Figure 7), and an explanation for this might be that the processes governing winter precipitation for these catchments are more regional (low pressure in the China Sea) compared with the wet summer monsoon circulation.

[31] Since objective functions were summarized for all indices, or for wet and dry patterns with MOFRBC, the optimum setting was not optimal for all indices. The poor results for Laoyukou concerning  $SS_{(C)RPS}$  indicated that the four statistical-downscaling methods we tested did not work well for the STARDEX indices with the selected predictor settings for this region. SDSMh performed fairly well, indicating that local processes are much more important for precipitation properties than the large-scale circulation. This points to the difficulty in optimizing the weather patterns for both dry and wet conditions. The relatively

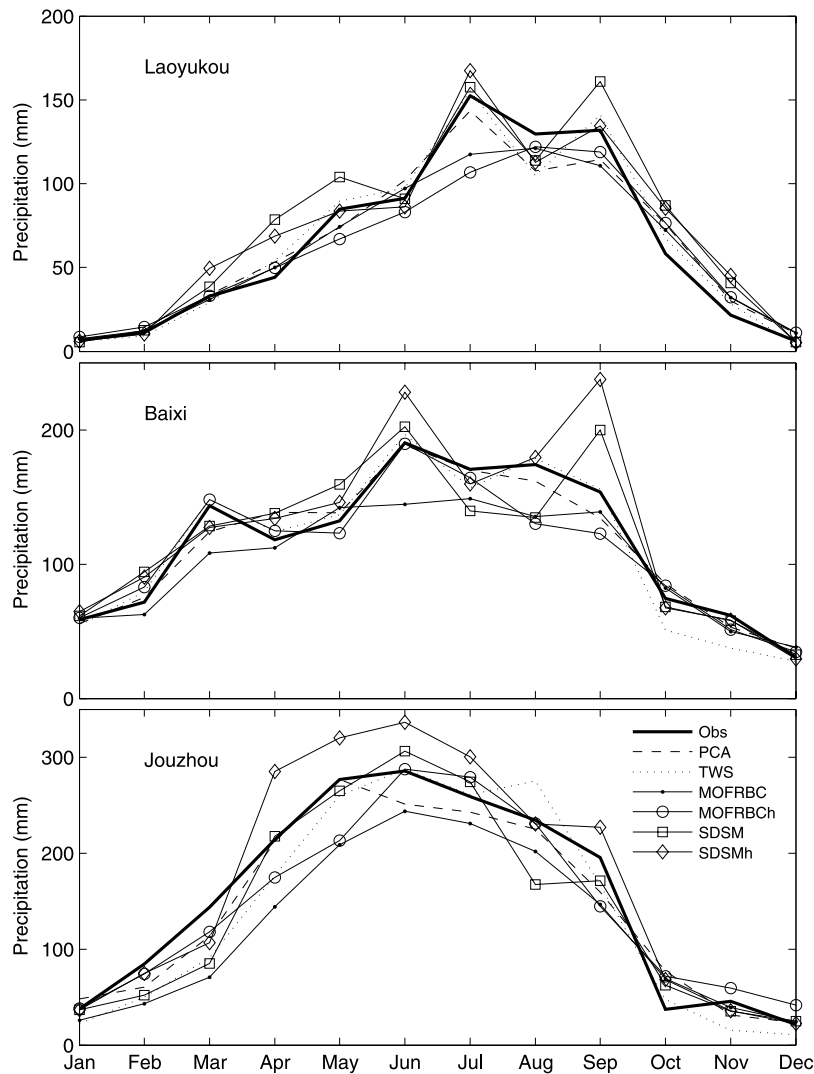


**Figure 5.** Observed and simulated monthly precipitation averaged over the validation period.

poor performance for *max5* during winter season (Figure 7) for the southerly catchments indicated that the methods were not so sensitive to heavy precipitation occurrences during this season. The same was seen in *maxdry* for summer, especially at Jouzhou. An explanation could be that heavy precipitation during the dry winter monsoon and long dry spells during the wet summer monsoon are rather rare events.

[32] The overall performance of SDSMh and MOFRBCh were slightly improved (Figure 7) compared with SDSM and MOFRBC, except for MOFRBCh at Baixi for the summer season. The poor performance of *90amount* for MOFRBCh in summer season for Jouzhou (Figure 7) was also reflected in the STARDEX indices (Table 4). The inclusion of humidity increased the number of days with intermediate precipitation. Other indices, such as *wetday* and *maxdry*, were better captured with humidity flux included in the predictor set than with MSLP only.

### 5.3. Timing and Amount of Precipitation

[33] The  $SS_{RPS}$  indicated that daily precipitation for Baixi catchment was generally best downscaled and that the SDSMh was most successful for all areas and seasons,

although MOFRBCh also outperformed the analogue methods. The results indicated that *RPS* can be a useful indicator for measuring precipitation extreme events if the thresholds are selected to analyze large precipitation amounts.

[34] The introduction of specific humidity enhanced the intra-annual variation for SDSM and MOFRBC (Figure 5). The inclusion of moisture flux shifted the precipitation toward intermediate precipitation amounts, which was also seen in the STARDEX indices. The method, however, was optimized to downscale extreme events, so the annual cycle could be improved with a different optimization. It could also be other local phenomena, such as late summer cyclones, that deliver much of the precipitation during this period. For Jouzhou the MOFRBCh increased the monthly totals at the same time as *wetday* and *90perc* decreased compared with MOFRBC, indicating a shift in the precipitation distribution toward more wet days with less precipitation when moisture flux was included. This indicated that the moisture flux corrected the bias in the wet summer indices, and did so for all catchments.

[35] *RPS* were consistently lower for the analogue methods (Table 5), which indicated that MOFRBCh and SDSMh were more responsive to the daily variations in the predic-

**Table 5.** Ranked-Probability Scores for Daily Precipitation and Seasonal Correlation of Total Precipitation of Downscaled Precipitation During the Validation Period 1979–1993 Over All Precipitation Stations in Each Catchment<sup>a</sup>

	PCA	TWS	MOFRBC	MOFRBCh	SDSM	SDSMh
<i>Laoyukou</i>						
Winter (Oct–Mar)						
SS <sub>RPS</sub>	8	31	35	35	44	43
$\rho_{FP}$	-0.22	0.57	0.02	0.05	0.45	0.65
Summer (Apr–Sep)						
SS <sub>RPS</sub>	24	33	41	42	49	50
$\rho_{FP}$	-0.04	0.72	-0.16	-0.10	0.67	0.73
<i>Baixi</i>						
Winter (Oct–Mar)						
SS <sub>RPS</sub>	14	25	43	49	54	52
$\rho_{FP}$	0.25	0.40	0.12	0.72	0.71	0.75
Summer (Apr–Sep)						
SS <sub>RPS</sub>	22	19	45	48	48	48
$\rho_{FP}$	0.25	0.40	0.12	0.72	0.71	0.75
<i>Jouzhou</i>						
Winter (Oct–Mar)						
SS <sub>RPS</sub>	7	22	32	37	41	42
$\rho_{FP}$	0.07	0.51	0.62	0.81	0.89	0.81
Summer (Apr–Sep)						
SS <sub>RPS</sub>	18	22	40	43	46	47
$\rho_{FP}$	0.49	0.50	0.67	0.82	0.46	0.57

<sup>a</sup>Probability scores are multiplied by 100.

tors. Even though this study focused on daily precipitation, it is important for the methods to be able to cope with the interannual variability sufficiently if they are expected to render reasonable results for years with different climate. Taking humidity into account in the methods clearly increased the seasonal correlation for all catchments during summer and for most catchments during winter season (Table 5). The seasonal correlation for MOFRBCh increased with decreasing latitude, and this together with the fact that *wetday* and *max5* were best downscaled for Baixi and Jouzhou indicated that the summer monsoon precipitation was best captured with this method.

[36] The spatial correlation of precipitation series within each catchment showed quite weak decline with distance (Figure 6). The MOFRBC includes spatial correlation in the precipitation model (equation (7)), a feature that is missing in the SDSM since it models each station separately, and the correlation was on par with the analogue methods. The spatial correlation between stations was preserved with the analogue methods, which also was expected since the spatial dependence between stations is kept intact with this method. The ability to correctly model the spatial correlation of precipitation is important for hydrological reasons, since flooding often is caused by heavy precipitation over large areas. In this sense the MOFRBC clearly has an advantage over the single-site version of SDSM. However, a more stringent comparison would be to compare MOFRBC with a multisite configuration of SDSM as was done by *Wilby et al.* [2003].

[37] The geographical difference between areas in terms of spatial correlation, especially in summer, is difficult to interpret. It does not seem to have any relationship to latitude or closeness to the sea. It might be local effects influencing the stations during winter. The correlation is higher during summer because of more rain during the

monsoon period, and thus more days with rain at all stations at the same time.

### 6. Conclusions

[38] In this study, four statistical downscaling methods were evaluated and their skills in downscaling daily precipitation amount and other characteristics were compared on

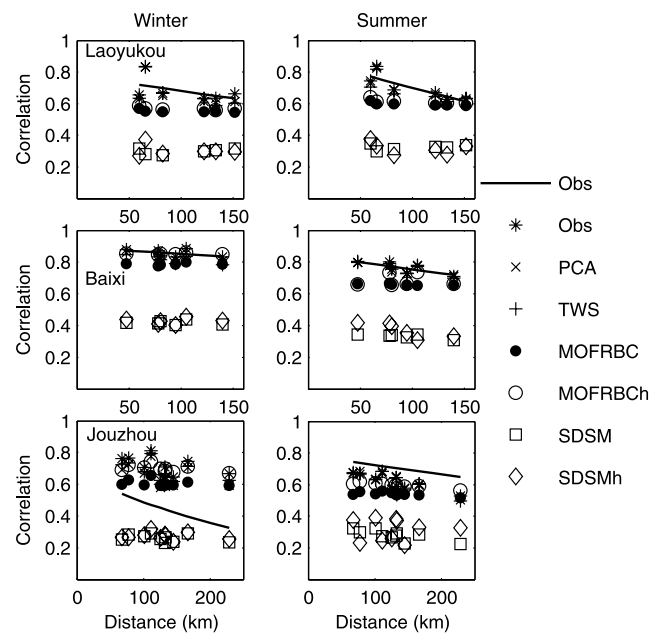


**Figure 6.** Spatial correlation of daily precipitation between pairs of stations plotted against distance between the stations. The solid lines represent a fitted exponential decay of the observed values.

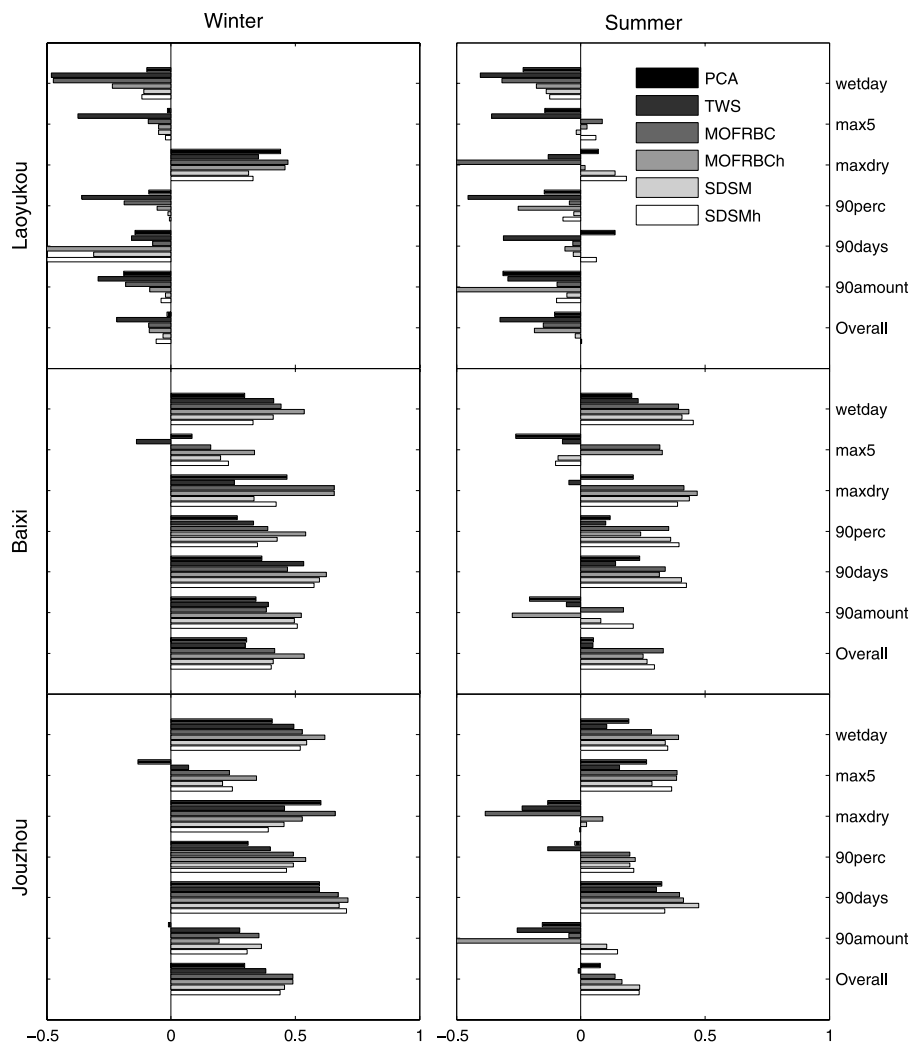


**Figure 7.**  $SS_{(C)RPS}$  for the STARDEX indices over the validation period.

three catchments in China, representing three climatic regions. It is concluded from the study that (1) for the subtropical monsoon region in southern China (Jouzhou) the SDSMh and SDSM methods performed best in summer season, and MOFRBCh method performed better in winter; (2) for the intermediate monsoon region in eastern region (Baixi) the MOFRBCh and MOFRBC performed best in summer season and the MOFRBCh method performed best in winter; and (3) for inland China the SDSMh method performed best for summer season and SDSM performed best for winter season. The analogue methods generally performed worse than the more sophisticated methods. The overall recommendation for any downscaling study, however, is to use an ensemble of methods, and this study supports this idea since no method was outstanding.

[39] The relationship between large-scale circulation and precipitation was strongest in the two southerly catchments, which also were more influenced by the monsoon than the central catchment. Winter precipitation was generally better captured than summer precipitation for the coastal stations. This study did not incorporate any known local processes, and more knowledge about these might improve the results for the Laoyukou catchment. The seasonal cycle was well captured for all methods. Including humidity improved the

overall results for most indices, especially for the interannual correlation of seasonal precipitation totals and the precipitation distribution. Humidity is therefore suggested as a key variable to use together with circulation variables for downscaling of precipitation in this part of China.

[40] **Acknowledgments.** Internal funding from Uppsala University and external funding from the Swedish Natural Science Research Council (contract G5301-972) and the Swedish Research Council (contract 621-2002-4352) made this work possible. Climate data were provided by the National Climate Centre of China, and the discharge data from Laoyukou, Baixi, and Jouzhou catchments were kindly supplied by Guoru Huang (Hohai University), Youpeng Xu (Nanjing University), and Yongqin Chen (Chinese University of Hong Kong), respectively. The Research Grants Council of the Hong Kong Special Administrative Region, China (Project CUHK4188/98H) partially supported the study. The authors also thank three anonymous reviewers and Robert Wilby for their useful comments on this paper.

## References

- Bárdossy, A., and E. J. Plate (1992), Space-time model for daily rainfall using atmospheric circulation patterns, *Water Resour. Res.*, *28*, 1247–1259.
- Bárdossy, A., L. Duckstein, and I. Bogardi (1995), Fuzzy rule-based classification of atmospheric circulation patterns, *Int. J. Climatol.*, *15*, 1087–1097.
- Bárdossy, A., J. Stehlik, and H.-J. Caspary (2001), Generating of areal precipitation series in the Upper Neckar Catchment, *Phys. Chem. Earth Part B*, *26*, 683–687.

- Beckmann, B.-R., and T. A. Buishand (2002), Statistical downscaling relationships for precipitation in the Netherlands and north Germany, *Int. J. Climatol.*, *22*(1), 15–32.
- Chen, D., and Y. Chen (2003), Association between winter temperature in China and upper air circulation over East Asia revealed by canonical correlation analysis, *Global Planet. Change*, *37*, 315–325.
- Chen, D., C. Achberger, J. Räisänen, and C. Hellström (2006), Using statistical downscaling to quantify the GCM-related uncertainty in regional climate change scenarios: A case study of Swedish precipitation, *Adv. Atmos. Sci.*, *23*(1), 54–60.
- Ding, Y. H. (1994), *Monsoons Over China*, 419 pp., Springer, New York.
- Durman, C. F., J. M. Gregory, D. C. Hassell, R. G. Jones, and J. M. Murphy (2001), A comparison of extreme European daily precipitation simulated by a global and a regional climate model for present and future climates, *Q. J. R. Meteorol. Soc.*, *127*, 1005–1015.
- Epstein, E. S. (1969), A scoring system for probability forecasts of ranked categories, *J. Appl. Meteorol.*, *8*, 985–987.
- Fan, L., C. Fu, and D. Chen (2006), A survey on statistical downscaling in climate studies (in Chinese with English abstract), *Adv. Earth Sci.*, *20*, 320–329.
- Frei, D. (2001), Statistical and Regional Dynamical Downscaling of Extremes for European Regions (STARDEX): Deliverable 11—Recommendations on variables and extremes for which downscaling is required, Eur. Comm., Brussels, Belgium. (Available at [http://www.cru.uea.ac.uk/projects/star dex/deliverables/D11/D11\\_synthesis.pdf](http://www.cru.uea.ac.uk/projects/star dex/deliverables/D11/D11_synthesis.pdf))
- Hanssen-Bauer, I., C. Achberger, R. Benestad, D. Chen, and E. Førland (2005), Empirical-statistical downscaling of climate scenarios over Scandinavia: A review, *Clim. Res.*, *29*, 255–268.
- Hellström, C., D. Chen, C. Achberger, and J. Räisänen (2001), A comparison of climate change scenarios for Sweden based on statistical and dynamical downscaling of monthly precipitation, *Clim. Res.*, *19*, 45–55.
- Hersch, H. (2000), Decomposition of the continuous ranked probability score for ensemble prediction systems, *Weather Forecasting*, *15*, 559–570.
- Jia, L., W. Li, and D. Chen (2006), A monthly atmospheric circulation classification and its relationship with climate in Harbin (in Chinese with English abstract), *Acta Meteorol. Sinica*, *64*(2), 236–245.
- Jolliffe, I., and D. B. Stephenson (Eds.) (2003), *Forecast Verification: A Practitioner's Guide in Atmospheric Science*, 254 pp., John Wiley, Hoboken, N. J.
- Kalnay, E., et al. (1996), NCEP/NCAR 40-year reanalysis project, *Bull. Am. Meteorol. Soc.*, *77*, 437–471.
- Liao, Y., Q. Zhang, and D. Chen (2004), Stochastic modeling of daily precipitation in China, *J. Geogr. Sci.*, *14*(4), 417–426.
- Linderson, M.-L., C. Achberger, and D. Chen (2004), Statistical downscaling and scenario construction of precipitation in Scania, southern Sweden, *Nord. Hydrol.*, *35*, 261–278.
- Murphy, A. H. (1971), A note on the ranked probability score, *J. Appl. Meteorol.*, *10*, 155–156.
- Obled, C., G. Bontron, and R. Garçon (2002), Quantitative precipitation forecasts: A statistical adaptation of model outputs through an analogues sorting approach, *Atmos. Res.*, *63*, 303–324.
- Samel, A., W.-C. Wang, and X.-Z. Liang (1999), The monsoon rainband over China and relationships with the Eurasian circulation, *J. Clim.*, *12*, 115–131.
- Simmonds, I., D. Bi, and P. Hope (1999), Atmospheric water vapor flux and its association with rainfall over China in summer, *J. Clim.*, *12*, 1353–1367.
- STARDEX (2001), Statistical and Regional Dynamical Downscaling of Extremes for European Regions: Description of work, Eur. Comm., Brussels, Belgium. (Available at <http://www.cru.uea.ac.uk/projects/star dex/description.pdf>)
- Stehlik, J., and A. Bárdossy (2002), Multivariate stochastic downscaling model for generating daily precipitation series based on atmospheric circulation, *J. Hydrol.*, *256*, 120–141.
- Stehlik, J., and A. Bárdossy (2003), Statistical comparison of European circulation patterns and development of a continental scale classification, *Theor. Appl. Climatol.*, *76*, 31–46.
- Wetterhall, F., S. Halldin, and C.-Y. Xu (2005), Statistical precipitation downscaling in central Sweden with the analogue method, *J. Hydrol.*, *360*, 174–190.
- Wetterhall, F., S. Halldin, and C. Y. Xu (2006), Seasonality properties of four statistical-downscaling methods in central Sweden, *Theor. Appl. Climatol.*, doi:10.1007/s00704-005-0223-3, in press.
- Wilby, R. L., and T. M. L. Wigley (1997), Downscaling general circulation model output: A review of methods and limitations, *Prog. Phys. Geogr.*, *21*, 530–548.
- Wilby, R. L., and M. D. Dettinger (2000), Streamflow changes in the Sierra Nevada, California, simulated using a statistically downscaled general circulation model scenario of climate change, in *Linking Climate Change to Land Surface Change*, pp. 99–121, Springer, New York.
- Wilby, R. L., L. E. Hay, and G. H. Leavesley (1999), A comparison of downscaled and raw GCM output: Implications for climate change scenarios in the San Juan River Basin, Colorado, *J. Hydrol.*, *225*, 67–91.
- Wilby, R. L., C. W. Dawson, and E. M. Barrow (2002), SDSM—A decision support tool for the assessment of regional climate change impacts, *Environ. Modell. Software*, *17*, 147–159.
- Wilby, R. L., O. J. Tomlinson, and C. W. Dawson (2003), Multi-site simulation of precipitation by conditional resampling, *Clim. Res.*, *23*, 183–194.
- Wilks, D. S., and R. L. Wilby (1999), The weather generation game: A review of stochastic weather models, *Prog. Phys. Geogr.*, *23*, 329–357.
- Xu, C.-Y. (1999), From GCMs to river flow: A review of downscaling methods and hydrologic modelling approaches, *Prog. Phys. Geogr.*, *23*, 229–249.
- Zorita, E., and H. von Storch (1999), The analogue method as a simple statistical downscaling technique: Comparison with more complicated methods, *Clim. J.*, *12*, 2474–2489.

A. Bárdossy, Institut für Wasserbau, Stuttgart University, Pfaffenwaldring 61, 70569 Stuttgart, Germany. (andras.bardossy@iws.uni-stuttgart.de)

D. Chen, Regional Climate Group, Earth Sciences Centre, Göteborg University, P.O. Box 460, 405 30 Göteborg, Sweden. (deliang@gvc.gu.se)

S. Halldin, Air and Water Science, Department of Earth Sciences, Uppsala University, 752 36 Uppsala, Sweden. (sven.halldin@hyd.uu.se)

F. Wetterhall, Swedish Meteorological and Hydrological Institute, SE-60176 Norrköping, Sweden. (fredrik.wetterhall@smhi.se)

C.-Y. Xu, Department of Geosciences, University of Oslo, P.O. Box 1047 Blindern, N-0316 Oslo, Norway. (chongyu.xu@geo.uio.no)